Supporting information for:

Synergistic optimization of triple phase junctions and oxygen vacancies over $Mn_xCd_{1-x}S$/Ov-WO_3 for boosting photocatalytic hydrogen evolution

Haitao Zhao [a,*], Hongjie Zhu [a,*], Min Wang [a], Heyuan Liu [b], Xiyou Li [c,*]

[a] Shandong Provincial Key Laboratory of Chemical Energy Storage and Novel Cell Technology, School of Chemistry and Chemical Engineering, Liaocheng University, Liaocheng, 252059, China. *E-mail:zhaohaitao_2014@163.com, zhuhongjie@lcu.edu.cn

[b] College of New Energy, China University of Petroleum (East China), Qingdao, Shandong, 266580, China

[c] School of Materials Science and Engineering, China University of Petroleum (East China), Qingdao, Shandong, 266580, China. * *E-mail: xiyouli@upc.edu.cn*

Characterization of Materials

X-ray diffraction (XRD) patterns of nanomaterials were recorded on a Rigaka Ultima IV diffractometer with Cu Kα radiation (λ = 1.538 Å). The morphologies of samples were investigated by field-emission scanning electron microscope (JEOL JSM-6700F) and transmission electron microscope (JEM 2100). X-ray photoelectron spectroscope (XPS) measurements were measured on a Thermo Escalab 250 Xi with Mg Kα as the excitation source. In situ XPS were performed under visible light irradiation. The UV/vis diffuse reflection spectra (DRS) were obtained on a Hitachi UV-3900 spectrophotometer with an integrated sphere attachment and $BaSO_4$ used as the reference. Steady-state fluorescence spectra, time resolved fluorescence spectra, and fluorescence quantum yields were measured with FLS980 (Edinburgh instrument Ltd, England). The absolute fluorescence quantum yields of all samples were obtained by using an integrating sphere and photoluminescence decay curves were measured on the single photon counting (TCSPC) mode. N_2 adsorption-desorption isotherms were measured at 77 K after heating the samples at 100°C for 5 h to remove any moisture and solvent molecules in the pore with a Beckman Coulter SA3100 analyzer. The Brunauer-Emmett-Teller (BET) method was utilized to calculate specific surface areas (S_{BET}). By using the Barrett-Joyner-Halenda model, the pore size and volume distributions were derived from the adsorption branches of isotherms.

Photocatalytic H_2 production experiment

The hydrogen evolution experiment was carried out in 250 mL quartz glass reaction flask containing 100 mL 0.25M Na_2S/0.35 M Na_2SO_3 solution and 10 mg photocatalyst. After 15 minutes of stirring, the air in the quartz bottle was completely removed by adding N_2 carrier gas. The reaction system was kept below 278 K by a cooling water bath. The reaction flask was placed in photocatalytic reaction system equipped with 300 Xe lamp (CEL-SPH2N) with UV-cutoff filter (λ ⩾ 420 nm) for hydrogen evolution reaction. The hydrogen production yield was detected through GC 7900 on-line gas chromatography with TCD detector. The active irradiation area of photoreactor is 16.5 cm^2. The stability of the photocatalyst was tested by continuous

hydrogen evolution experiments over 12 hours.

The apparent quantum yield (AQY) of photocatalyst at different wavelengths was measured by using different band filters (420 nm, 450 nm, 520 nm, 600 nm). The apparent quantum yield is calculated by the following formula：

$$AQY[\%] = \frac{number\ of\ reacted\ electrons}{number\ of\ incident\ photons} \times 100\%$$
$$= \frac{2 \times number\ of\ evolved\ H_2\ molecules}{number\ \ of\ incident\ photons} \times 100\% \qquad (1)$$

Photoelectrochemical measurements

The photoelectrochemical measurements were collected with Gamry Reference 600 workstation. The working electrode was prepared as follows: the 5 mg sample was dissolved in 2 mL ethanol solution with 10 μL of Nafion solution, and then coated on FTO conductive glass of 1 cm × 1 cm. 0.50 mol·L^{-1} Na_2SO_4 solution (electrolyte solution), Pt sheet electrode (counter electrode), Ag/AgCl electrode (reference electrode) and working electrode formed a three-electrode system. EIS was tested in a range of 0.01-10^5 Hz frequency with an amplitude of 10 mV. And linear sweep voltammetry (LSV) test voltage ranges from -2.0 to 0.5 V and scan rate of 0.05 V/s.

Computational details

Electronic structures of the t-MCS and Ov-WO_3 were investigated via the plane-wave-pseudopotential approach based on the density functional theory (DFT). Their electronic structures were calculated using the Cambridge serial total energy package (CASTEP) module. The Perdew-Burke-Ernzerhof (PBE) exchange-correlation functional was selected within the generalized gradient approximation (GGA). A cutoff energy of 450 eV was used. Through the BFGS-based method, the convergence tolerance for the energy change, force, maximum stress and maximum displacement tolerances were set at 1.0×10^{-5} eV/atom, 0.03 eV/Å, 0.05 GPa, and 1.0×10^{-3} Å, respectively. After geometry optimization, all the optimized models were adopted to conduct the density of state (DOS) and the calculated work functions for t-MCS and Ov-WO_3 model.

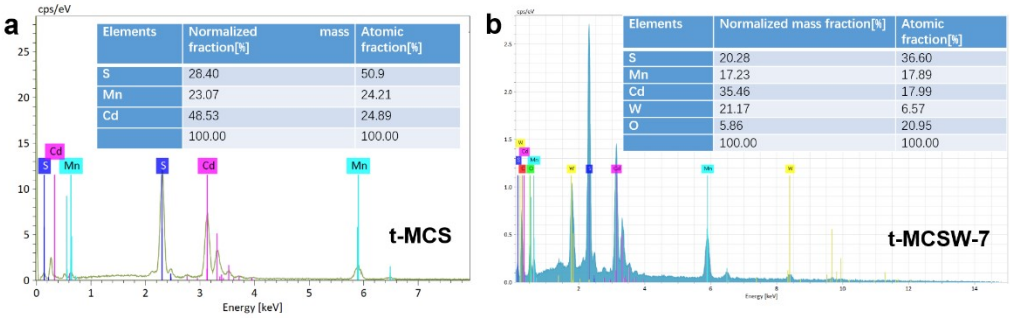

Fig. S1 EDS spectra and elements contents for t-MCS (a), t-MCSW-7 (b).

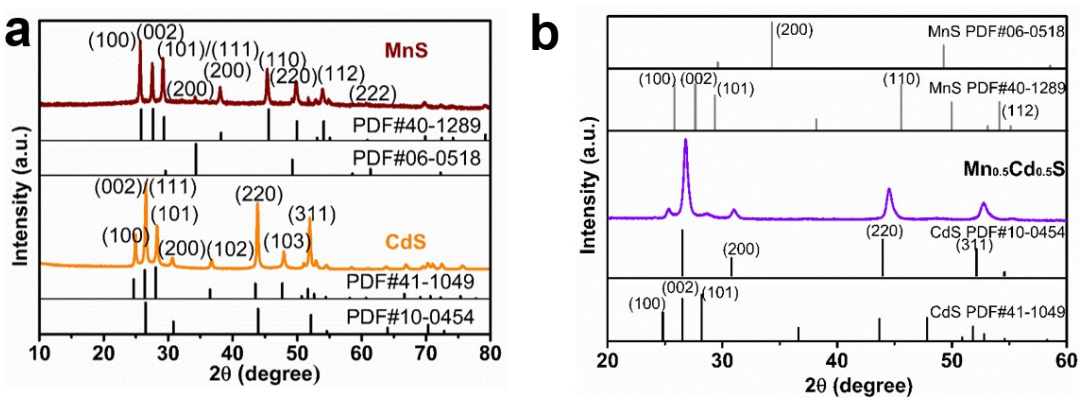

Fig. S2 Typical powder XRD diffraction patterns of (a) CdS, MnS, (b) nanotwin $Mn_{0.5}Cd_{0.5}S$.

Note: The as-prepared CdS exhibits characteristic peaks at 25.19°, 26.83°, 28.40°, 30.50°, 36.82°, 43.87°, 47.97°, and 52.28°, which are in exact agreement with (100), (002), (101), (102), (220), (103) facets of the hexagonal CdS (PDF # 41-1049) and (111), (200), (220) and (311) facets of cubic CdS (PDF # 10-0454), confirming that the existence of mixed-phase CdS.[41,42] Further analysis was conducted to determine the phase composition the prepared MnS. The XRD pattern of MnS reveals peaks at 2θ values of 25.60°, 27.52°, 29.30°, 34.15°, 38.46°, 45.51°, 49.89°, 54.08°, and 61.52°. These peaks demonstrate a remarkable alignment with the (100), (002), (101), (200), (110), and (112) crystal facets wurtzite MnS (PDF#40-1289) and (111), (200), (220) and (222) crystal planes cubic MnS (PDF#06-0518),[18,19] indicating that MnS is also a mixed phase.

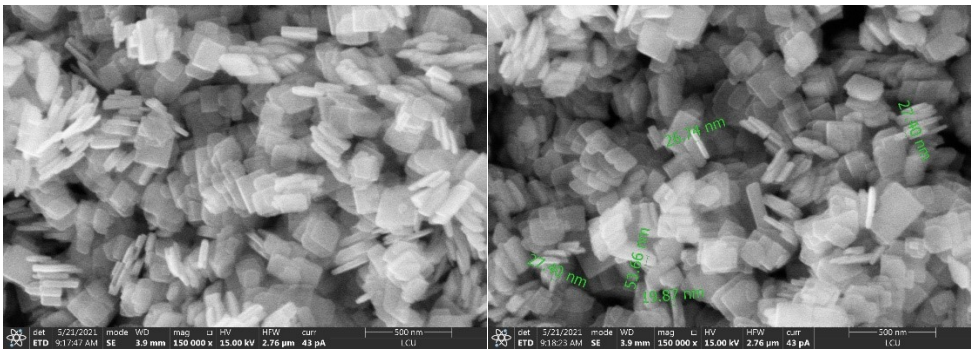

Fig. S3 SEM images of Ov-WO_3 nanosheets

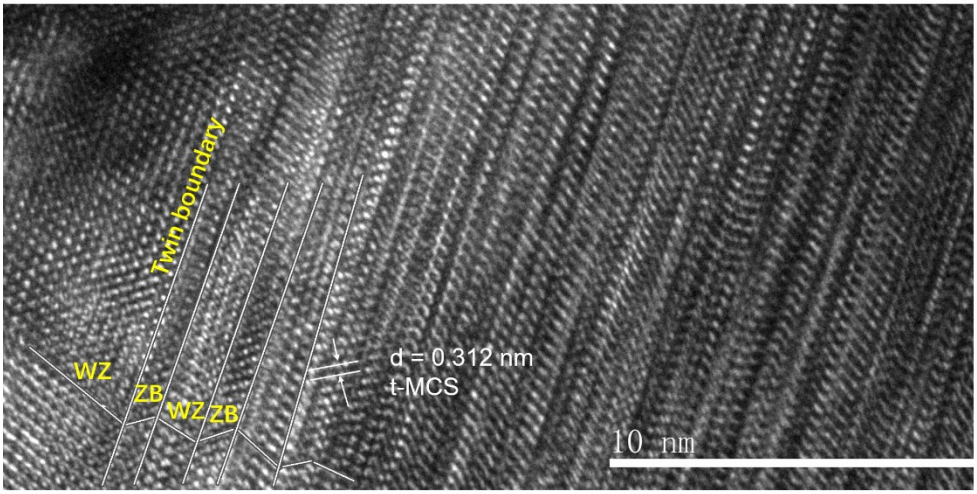

Fig. S4 HRTEM image of t-MCS.

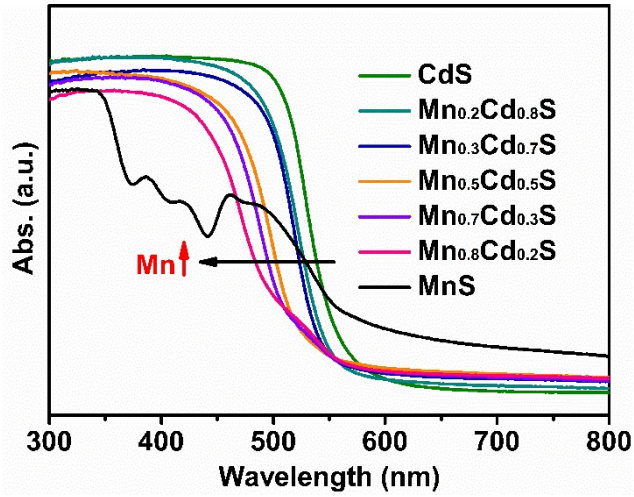

Fig. S5 UV-Vis DRS of nanotwin $Mn_xCd_{1-x}S$ samples.

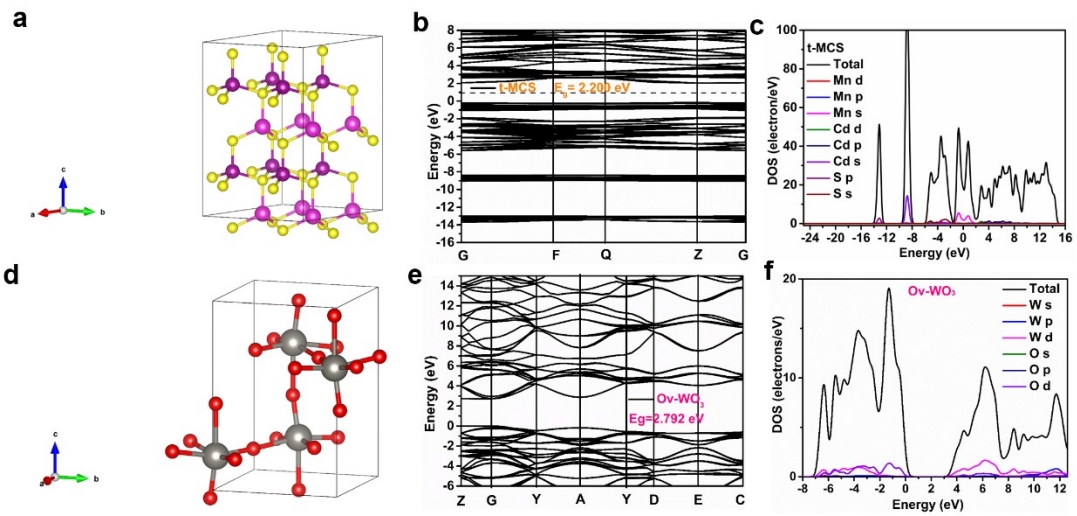

Fig. S6 Optimized geometric structure, band structure and density of states of t-MCS (002) (a, b, c), Ov-WO_3 (200) (d, e, f).

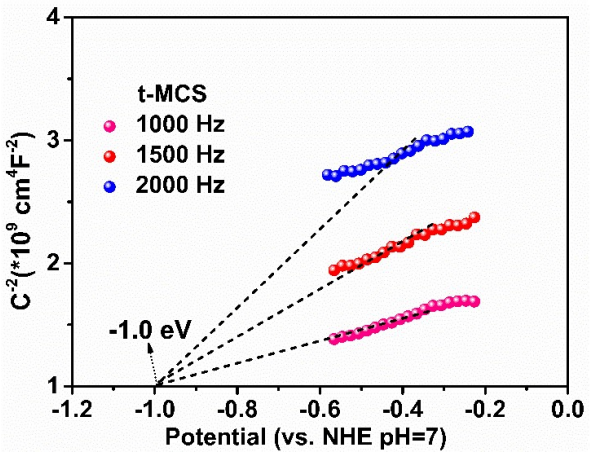

Fig. S7 The Mott-Schottky plots of t-MCS with different frequency.

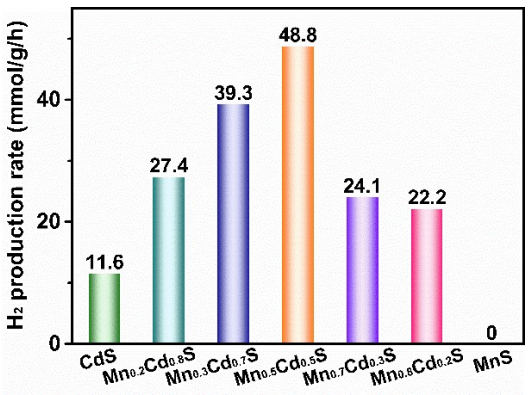

Fig. S8 The hydrogen evolution rate of nanotwin $Mn_xCd_{1-x}S$ samples.

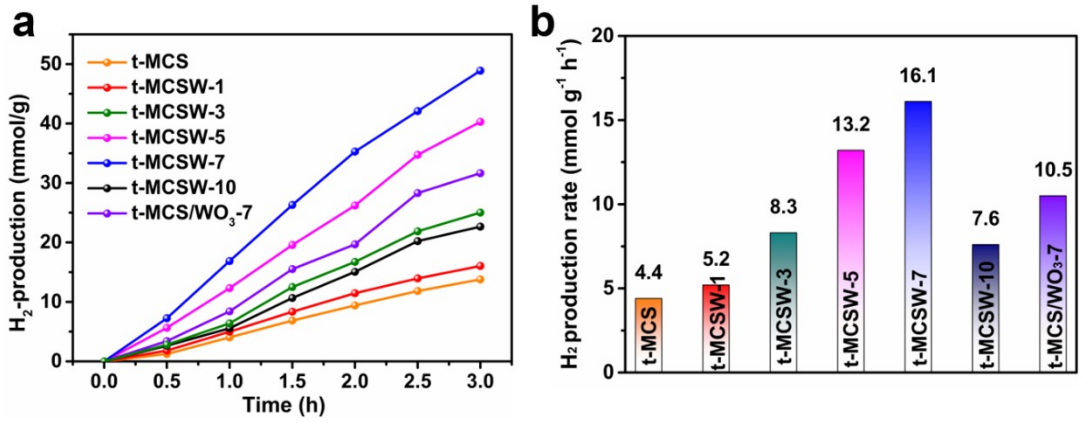

Fig. S9 The amount of hydrogen evolution (a) and hydrogen evolution rate (b) of t-MCS-x under λ > 510 nm irradiation.

Table S1 BET specific surface area, and BJH average pore diameter parameters of Ov-WO_3, WO_3, t-MCS and t-MCSW-7.

Samples	S_{BET} (m^2/g)	Ave pore size (nm)
Ov-WO_3	34.62	25.5
WO_3	11.95	32.5
t-MCS	6.87	29.4
t-MCSW-7	18.40	30.1

Table S2 Comparison of photocatalytic hydrogen evolution activity over $Mn_xCd_{1-x}S$-based catalysts.

Photocatalysts	Mass (mg)	Light source	Sacrificial agents	PHE (mmo $g^{-1}h^{-1}$)	H_2 rate (mmol h^{-1})
t-MCSW-7 In this work	10	300 W Xe lamp (λ > 420 nm)	100 ml H_2O 0.35 M Na_2S/0.25 M Na_2SO_3	194.1	1.941
$Mn_{0.5}Cd_{0.5}S$ twin [1]	5	300 W Xe lamp (λ > 400 nm)	100 ml H_2O 0.5 M Na_2S/0.5 M Na_2SO_3	16.48	0.082
$NiCo_2S_4$/T-MCS [2]	10	300 W Xe lamp (λ ≥420 nm)	100 ml H_2O 0.35 M Na_2S/0.25 M Na_2SO_3	127.3	1.273
NiS_x/T-MCS [3]	10	300 W Xe lamp (λ ≥ 420 nm)	100 ml H_2O 0.35 M Na_2S/0.25 M Na_2SO_3	111.5	1.115
$2MoO_2$/3Au/$Mn_{0.5}Cd_{0.5}S$ [4]	50	300 W Xe lamp	100 ml H_2O 0.1 M Na_2S/0.3 M Na_2SO_3	12.77	0.638
Fe_2P/P-$Mn_{0.5}Cd_{0.5}S$ [5]	30	300 W Xe lamp (λ ≥ 400 nm)	40 ml H_2O, Lactic acid (5 ml)	2.94	0.088

CoP/$Mn_{0.5}Cd_{0.5}S$ [6]	10	300 W Xe lamp (λ ≥ 420 nm)	20 ml H_2O, Lactic acid (8 ml)	42.95	0.429
g-C_3N_4/$Mn_{0.8}Cd_{0.2}S$ [7]	50	300 W Xe lamp (λ > 420 nm)	100 ml H_2O 0.1 M Na_2S/0.5 M Na_2SO_3	4	0.2
colloidal $Mn_{0.5}Cd_{0.5}S$ [8]	10	λ > 400 nm	80 ml H_2O 0.75 M Na_2S/1.05 M Na_2SO_3	26	0.26
$Mn_{0.25}Cd_{0.75}S$/$NiCo_2O_4$ [9]	40	300 W Xe lamp	90 ml H_2O, Lactic acid (10 ml)	61.16	2.446
Cu-MOFs/$Mn_{0.5}Cd_{0.5}S$ [10]	10	5W LED	30 ml H_2O 0.35 M Na_2S/0.25 M Na_2SO_3	10.95	0.109
Co_xP/$Mn_{0.35}Cd_{0.65}S$ [11]	40	300 W Xe lamp (λ ≥ 420 nm)	60 ml H_2O 0.35 M Na_2S/0.25 M Na_2SO_3	7.189	0.287
MoS_2/$Mn_{0.25}Cd_{0.75}S$ [12]	50	300 W Xe lamp (λ ≥ 420 nm)	30 ml H_2O 0.5 M Na_2S/0.5 M Na_2SO_3	12.47	0.624
$Ni(OH)_2$/$Mn_{0.3}Cd_{0.7}S$ [13]	5	300 W Xe lamp (λ ≥ 420 nm)	50 ml H_2O 0.25 M Na_2S/0.35 M Na_2SO_3	71.09	0.355
NiSe/$Mn_{0.5}Cd_{0.5}S$ [14]	5	300 W Xe lamp (λ ≥ 420 nm)	50 ml H_2O 0.0175 M Na_2S/0.0125 M Na_2SO_3	28.08	0.140
$Cu_{2-x}S$/$Mn_{0.5}Cd_{0.5}S$/MoS_2 [15]	50	300 W Xe lamp (λ ≥ 420 nm)	100ml H_2O 0.35 M Na_2S/0.25 M Na_2SO_3	13.75	0.688

The average fluorescence lifetime (τ_{ave}) can be calculated using the equation:

$$\tau_{ave} = (A_1{\tau_1}^2 + A_2{\tau_2}^2)/(A_1\tau_1 + A_2\tau_2) \qquad \text{(S1)}$$

Table S3 Lifetime constant τ_i and quantum yield Φ of t-MCS, Ov-WO_3, and t-MCSW-7.

Samples	τ(ns)	τ_{ave}(ns)	χ^2	Φ(%)
t-MCS	τ_1 = 0.7260 (44.70%) τ_2 = 8.3072 (55.30%)	7.806	1.320	1.33%
Ov-WO_3	τ_1 = 0.7426 (48.27%) τ_2 = 8.8142 (51.73%)	8.226	1.255	0.38%
t-MCSW-7	τ_1 = 0.6748 (38.11%) τ_2 = 9.2484 (61.89%)	8.879	1.296	0.31%

References

[1] H. Huang, Z. Wang, B. Luo, P. Chen, T. Lin, M. Xiao, S. Wang, B. Dai, W. Wang, J. Kou, C. Lu, Z. Xu, L. Wang, Design of twin junction with solid solution interface for

efficient photocatalytic H_2 production, *Nano Energy*, 2020, 69, 104410-104419.

[2] C. Wang, X. Ma, Z. Fu, X. Hu, J. Fan, E. Liu, Highly efficient photocatalytic H_2 evolution over $NiCo_2S_4/Mn_{0.5}Cd_{0.5}S$: Bulk twinned homojunctions and interfacial heterojunctions, *Journal of Colloid and Interface Science*, 2021, 592, 66-76.

[3] Z. Wang, M. Li, J. Li, Y. Ma, J. Fan, E. Liu, NiS_x modified $Mn_{0.5}Cd_{0.5}S$ twinned homojunctions for efficient photocatalytic hydrogen evolution, *Journal of Environmental Chemical Engineering*, 2022, 10, 107375-107384.

[4] Y. Liu, L. Wang, H. Lv, X. Wu, X. Xing, S. Song, Constructing robust $MoO_2/Au/Mn_{0.5}Cd_{0.5}S$ multiple heterojunctions for improved photocatalytic hydrogen evolution: An insight into the synergetic effect of MoO_2 and Au cocatalysts, *Applied Surface Science*, 2021, 541, 148582-148592.

[5] Y. Liu, J. Yan, D. Liu, L. Shi, The highly efficient photocatalytic hydrogen evolution of $Mn_{0.5}Cd_{0.5}S$ by synergistic effect of Fe_2P and P doping, *Journal of Alloys and Compounds*, 2023, 938, 168545-168554.

[6] M. Xiong, Y. Qin, B. Chai, J. Yan, G. Fan, F. Xu, C. Wang, G. Song, Unveiling the role of Mn-Cd-S solid solution and MnS in $Mn_xCd_{1-x}S$ photocatalysts and decorating with CoP nanoplates for enhanced photocatalytic H_2 evolution, *Chemical Engineering Journal*, 2022, 428, 131069-131079 .

[7] H. Liu, Z. Xu, Z. Zhang, D. Ao, Novel visible-light driven $Mn_{0.8}Cd_{0.2}S/g\text{-}C_3N_4$ composites: Preparation and efficient photocatalytic hydrogen production from water without noble metals, *Applied Catalysis A: General*, 2016, 518, 150-157.

[8] L. Li, G. Liu, S. Qi, X. Liu, L. Gu, Y. Lou, J. Chen, Y. Zhao, Highly efficient colloidal $Mn_xCd_{1-x}S$ nanorod solid solution for photocatalytic hydrogen generation, *Journal of Materials Chemistry A*, 2018, 6, 23683-23689.

[9] T. Feng, H. Li, R. Gao, G. Su, W. Wang, B. Dong, L. Cao, Manganese Cadmium Sulfide Nanoparticles Solid Solution on Cobalt Acid Nickel Nanoflakes: A Robust Photocatalyst for Hydrogen Evolution, *ChemSusChem*, 2022, 15, 202200288-202200298.

[10] Y. Cao, G. Wang, H. Liu, Y. Li, Z. Jin, Q. Ma, Regular octahedron Cu-MOFs modifies $Mn_{0.05}Cd_{0.95}S$ nanoparticles to form a S-scheme heterojunction for

photocatalytic hydrogen evolution, *International Journal of Hydrogen Energy*, 2021, 46, 7230-7240.

[11] X. He, D. Zeng, Y. Liu, Q. Chen, J. Yang, R. Gao, T. Fujita, Y. Wei, Porous Co_xP nanosheets decorated $Mn_{0.35}Cd_{0.65}S$ nanoparticles for highly enhanced noble-metal-free photocatalytic H_2 generation, *Journal of Colloid and Interface Science*, 2022, 625, 859-870.

[12] Q.-Z. Huang, Y. Xiong, Q. Zhang, H.-C. Yao, Z.-J. Li, Noble metal-free MoS_2 modified $Mn_{0.25}Cd_{0.75}S$ for highly efficient visible-light driven photocatalytic H_2 evolution, *Applied Catalysis B: Environmental*, 2017, 209, 514-522.

[13] J. Zhang, C. Cheng, F. Xing, C. Chen, C. Huang, 0D β-$Ni(OH)_2$ nanoparticles/1D $Mn_{0.3}Cd_{0.7}S$ nanorods with rich S vacancies for improved photocatalytic H_2 production, *Chemical Engineering Journal*, 2021, 414, 129157-129163.

[14] X. Jiang, H. Gong, Q. Liu, M. Song, C. Huang, In situ construction of NiSe/$Mn_{0.5}Cd_{0.5}S$ composites for enhanced photocatalytic hydrogen production under visible light, *Applied Catalysis B: Environmental*, 2020, 268, 118439-118449 .

[15] X. Liu, Q. Liu, P. Wang, Y. Liu, B. Huang, E.A. Rozhkova, Q. Zhang, Z. Wang, Y. Dai, J. Lu, Efficient photocatalytic H_2 production via rational design of synergistic spatially-separated dual cocatalysts modified $Mn_{0.5}Cd_{0.5}S$ photocatalyst under visible light irradiation, *Chemical Engineering Journal*, 2018, 337, 480-487.